Tian Yi Ma, Sheng Dai and Shi Zhang Qiao
**Self-supported electrocatalysts for advanced energy conversion processes**
Materials Today, 2016; 19(5):265-273



Originally published at:
http://doi.org/10.1016/j.mattod.2015.10.012

ELSEVIER



# Self-supported electrocatalysts for advanced energy conversion processes

**Tian Yi Ma, Sheng Dai and Shi Zhang Qiao***

School of Chemical Engineering, The University of Adelaide, Adelaide, SA 5005, Australia

**The biggest challenge in developing new energy conversion technologies such as rechargeable metal-air batteries, regenerated fuel cells and water splitting devices is to find suitable catalysts that can efficiently and stably catalyze the key electrochemical processes involved. This paper reviews the new development of self-supported electrocatalysts in three categories: electrocatalysts growing on rigid substrates, electrocatalysts growing on soft substrates, and free-standing catalyst films. They are distinct and superior to the conventional powdery electrocatalysts, showing advantages in controllable nanostructure and chemical component, flexible electrode configuration, and outstanding catalytic performance. The self-supported electrocatalysts with various architectures like nanowire/plate/pillar arrays and porous films, composed of metals, metal oxides/selenides/phosphides, organic polymers, carbons and their corresponding hybrids, are presented and discussed. These catalysts exhibit high activity, durability and selectivity toward oxygen reduction, oxygen evolution, and/or hydrogen evolution reactions. The perspectives on the relevant areas are also proposed.**

## Introduction

Nowadays, global concerns have been concentrated on the utilization of clean and sustainable energy as the alternative of fossil fuels due to the aggravating energy crisis and environmental issues. Many advanced devices involving electrochemical processes for clean energy conversion are being extensively investigated by both experimental and theoretical methods [1–4], and their performance is significantly influenced by the kinetics of key electrocatalytic reaction processes, such as the oxygen reduction reaction (ORR), oxygen evolution reaction (OER), and hydrogen evolution reaction (HER) [5–8]. In the past decades, a large variety of highly efficient electrocatalysts have been developed to accelerate the commercialization of these energy conversion devices [9–15], driven by profound understanding on the nature of relevant electrocatalytic processes and by technological advances in the relevant fields. However, the conventional electrocatalysts for ORR, OER and HER, used under experimental conditions and in realistic devices, are usually in the form of fine powders. Electrode fabrication always requires the time-consuming film casting or coating procedure with assistance of polymeric binders and extra conductive additives, which results in uncontrolled microstructures, limited active surface areas, plenty of dead volumes and undesirable interface that are unfavorable for electron conductance and multiphase reactant/product mass transport [16–18]. Moreover, continuous gas evolution (i.e. $H_2$, $O_2$) during such electrocatalytic reactions makes the coated catalysts peel off from electrodes [19,20], which greatly impairs their catalytic activity and lifetime (Fig. 1).

Recently, self-supported electrocatalysts directly growing on conductive substrates or forming free-standing films have attracted tremendous interest [21,22]. This new class of electrocatalysts exhibits outstanding performance for the ORR, OER and/or HER processes with many intrinsic advantages in comparison with their powdery counterparts (Fig. 1). Basically, through different synthetic strategies such as hydrothermal process or electrochemical deposition, electroactive species are able to *in situ* grow on rigid metallic substrates or flexible carbonaceous substrates in the fashion of nanostructured arrays, or form free-standing films with three-dimensional (3D) porous structures [23–26]. The one-pot fabrication protocol without post-coating procedure does not

*Corresponding author:. Qiao, S.Z. (s.qiao@adelaide.edu.au)

 http://dx.doi.org/10.1016/j.mattod.2015.10.012

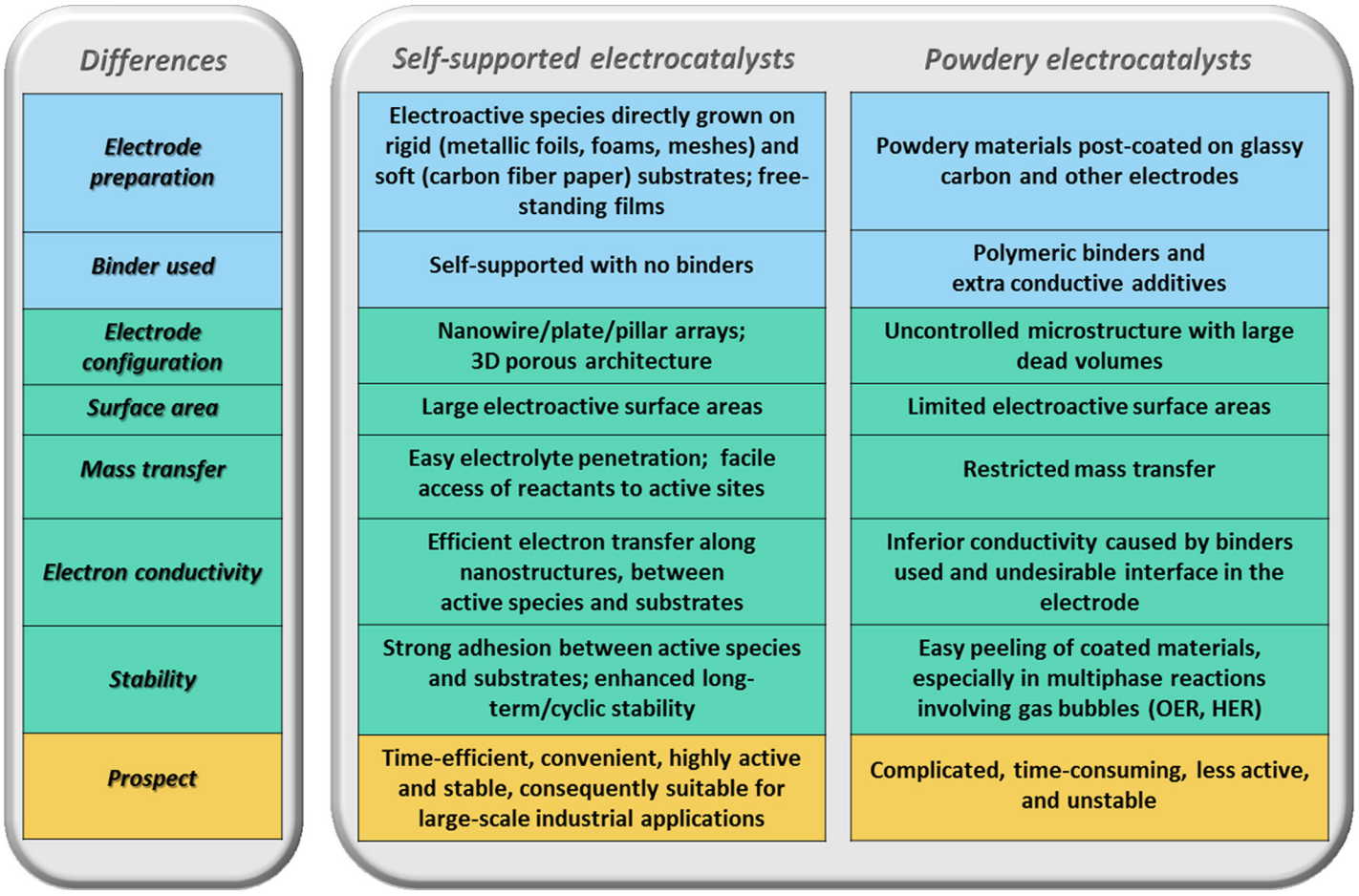


**FIGURE 1**

A comparison between self-supported and powdery electrocatalysts.

require organic binders. It can lead to the direct contact of the electroactive species with underneath conductive substrates, and the well integrity of the free-standing catalyst films. This may assure the good electron conductivity and favor the high mechanical stability of catalysts for long-term and cyclic usage [27,28]. Also, the complex nanostructures of self-supported catalysts are more effective in enlarging the catalytically active surface areas as compared to conventional planar catalyst coatings, which benefits better exposure and enhanced utilization of electroactive sites [21–24]. Furthermore, the open space within nanostructured arrays or 3D porous films facilitates electrolyte penetration, ion (e.g. $OH^-$, $H^+$) diffusion to the electroactive sites, and the fast emission of reaction products (e.g. $O_2$, $H_2$), consequently promoting the reaction kinetics [25,26]. Thus, the self-supported electrocatalysts with time-efficient and convenient preparation procedure as well as excellent activity and stability have shown great potential for direct application in many clean energy devices.

Up to now, there are several comprehensive reviews on the development of electrocatalysts aiming at materials synthesis (mainly in powdery form) and catalytic applications [29–33]. Some reviews also introduce self-supported materials for energy storage in supercapacitors and lithium-ion batteries [34–36]. However, no detailed review focuses on the self-supported materials for electrocatalytic processes. The present review highlights the design and fabrication of various self-supported catalysts for key electrochemical reactions such as ORR, OER and HER. Three typical categories including electrocatalysts growing on rigid substrates, electrocatalysts growing on soft substrates, and free-standing catalyst films are presented and discussed, revealing the material structure, catalytic performance and their end-uses in practical devices.

## Electrocatalysts growing on rigid substrates

Metal foils are the most commonly used rigid substrates to cultivate electroactive species. Various metal oxides have been chosen as the electroactive species, in which spinel-phase cobalt oxides ($CoO_x$) are widely investigated due to their good catalytic activity and corrosion stability toward electrochemical reactions in alkaline media [37,38]. Initial studies afford irregular nanoparticles dispersed on metal foil surface without specific nanostructures. For instance, $CoO_x$ nanoparticles were grown on different metal foils including Au, Pd, Pt, Cu and Co by a galvanostatic deposition method [39]. The electroactivity toward OER decreased in the order of $CoO_x$/Au > $CoO_x$/Pt > $CoO_x$/Pd > $CoO_x$/Cu > $CoO_x$/Co, paralleling to the electronegativity drop of metal foils used. Notably, even without any subtle nanostructure, the turnover frequency (TOF) for OER occurring on $CoO_x$/Au (~1.8 $s^{-1}$) was nearly 40 times higher than that of bulk $CoO_x$, and three times higher than that of bulk Ir, the state-of-the-art noble metal OER electrocatalyst [40,41], which implies the superiority of self-supporting configurations.

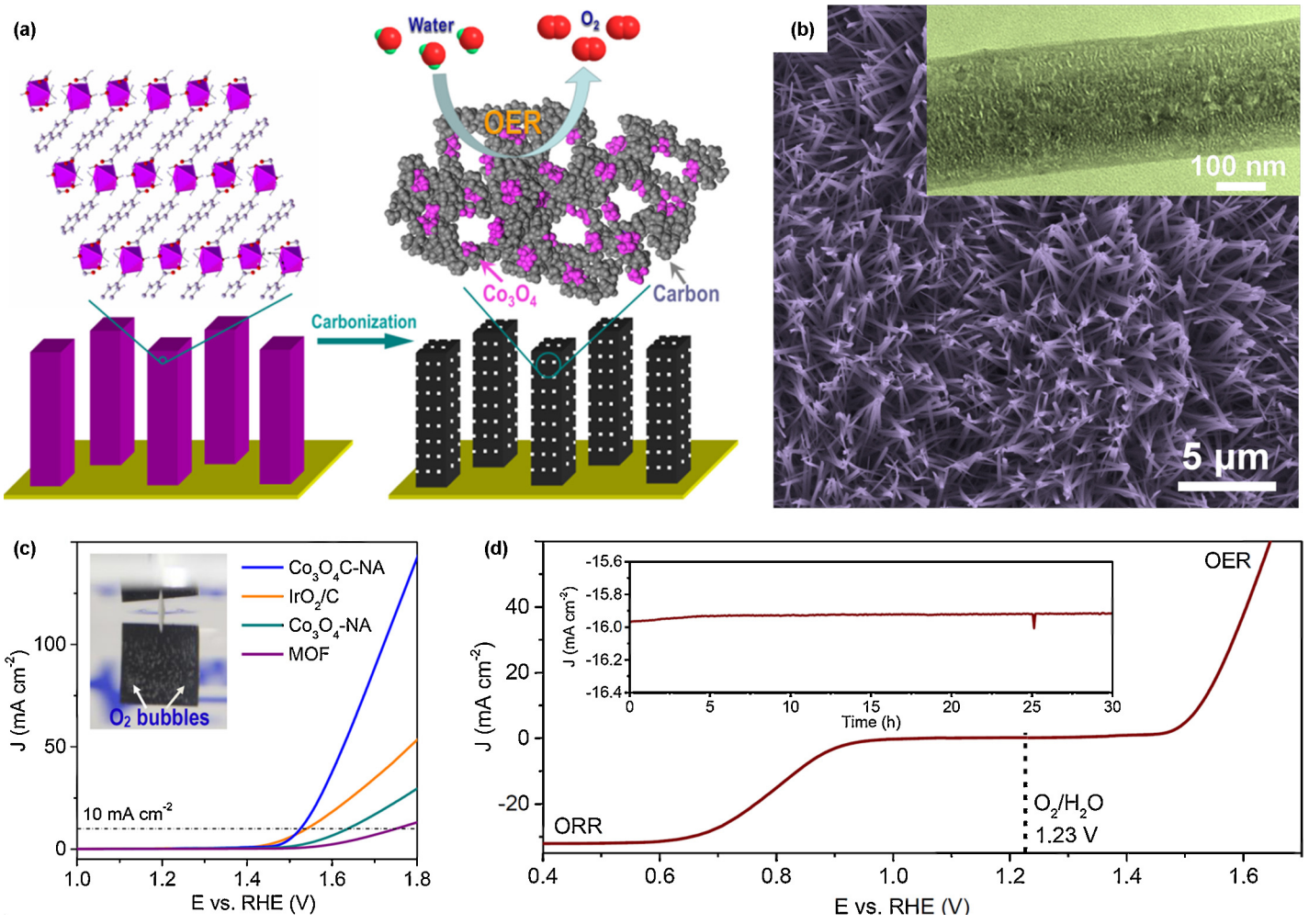


**FIGURE 2**

(a) Fabrication of $Co_3O_4$-carbon porous nanowire arrays ($Co_3O_4$C-NA). (b) SEM and (inset in panel b) TEM images of $Co_3O_4$C-NA. (c) Polarization curves and (inset in panel c) optical image of $Co_3O_4$C-NA directly used as the OER electrode operating at 1.70 V in 0.1 M KOH with bubbles on the surface indicating the formation of $O_2$ ($IrO_2$/C: $IrO_2$ supported on carbon powder, $Co_3O_4$-NA: pure $Co_3O_4$ nanowire arrays, MOF: metal-organic framework precursor). (d) Polarization curve in the whole region of OER and ORR, and (inset in panel d) chronoamperometric response of $Co_3O_4$C-NA at a constant potential of 0.78 V, with methanol addition after 25 hours. Reproduced from Ref. [44] with permission from the American Chemical Society.

Benefiting from the rapid development of nanotechnology, the morphology of active species on metal foils can be rationally designed. Using an ammonia-evaporation-induced growth strategy, Ni-doped $Co_3O_4$ ($Ni_xCo_{3-x}O_4$) nanowire (NW) arrays were grown on Ti foil, which could also be extended to other compositions such as Li-, Cu-, and Mn-doped $Co_3O_4$ NW arrays [42]. NW-derived morphologies can be obtained by further altering synthetic conditions. Liu *et al.* reported the preparation of hierarchical $Zn_xCo_{3-x}O_4$ structure on Ti foil by a hydrothermal process, which was composed of small secondary nano-needles being adhered to the primary rhombus-shaped pillar arrays [43], showing excellent OER activity, that is, a small overpotential of ~0.32 V to achieve a 10 mA cm$^{-2}$ current density with a Tafel slope of 51 mV decade$^{-1}$, comparable to the commercial Ir/C catalyst [40,41]. Basically, complex nanostructures directly growing on metal foils have many structural advantages. For example, the open space with large surface area is able to facilitate diffusion of reactive species; the advanced porosity with high roughness factor and active site density can accelerate surface reaction. These superiorities together lead to the excellent electroactivity of the obtained catalysts.

However, the aforementioned NW arrays are unexceptionally composed of semiconductive metal oxides, which cannot ensure the smooth electron transport along them [21–26]; and the mass transport and access to catalytically active sites are limited due to the low porosity of individual NWs [42,43]. To overcome these drawbacks, hybrid porous NW arrays consisting of strongly interacting $Co_3O_4$ and carbon ($Co_3O_4$C-NA) were synthesized by carbonizing the metal-organic framework (MOF) NWs growing on Cu foil (Fig. 2a) [44]. Due to the deterioration and carbonization of alternating naphthalene layers in the MOF precursor [45,46], the resulting catalysts possessed numerous slit-like pores throughout the NWs (Fig. 2b), showing a high surface area of 251 m$^2$ g$^{-1}$, which was much higher than the NW arrays prepared from inorganic precursors (<100 m$^2$ g$^{-1}$) [21–26,42,43]. This novel self-supported catalysts could be used in alkaline solutions, affording a low onset overpotential of 0.24 V for OER and a stable 10.0 mA cm$^{-2}$ current density at an overpotential of 0.29 V for 30 hours in 0.1 M KOH with a high Faradaic efficiency of 99.3% (Fig. 2c). Its outstanding electroactivity, better than those of pure $Co_3O_4$ NWs, the MOF precursor and $IrO_2$/C, can be attributed to the unique NW

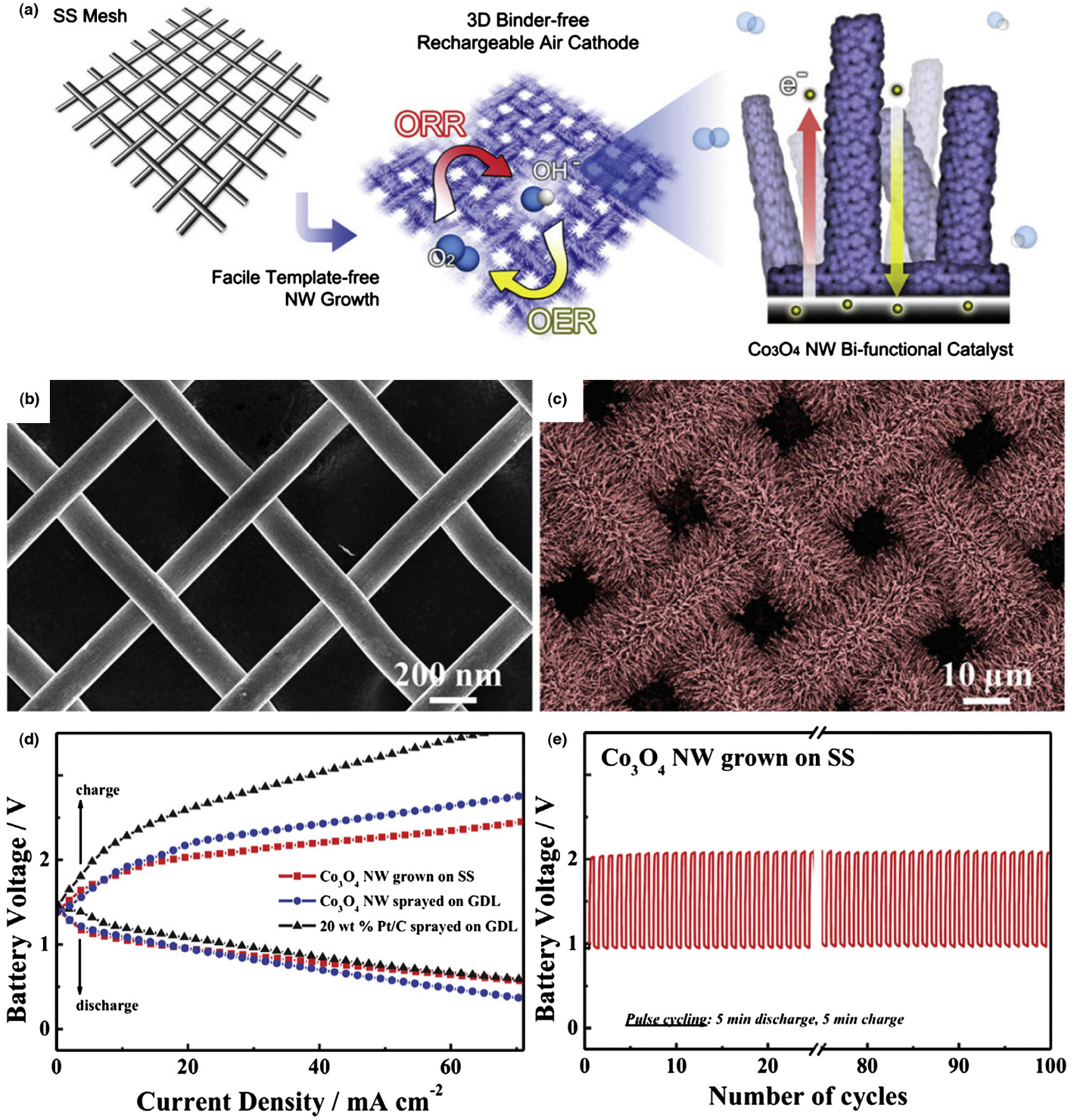


**FIGURE 3**

(a) Schematic illustration of the growth of $Co_3O_4$ NWs for bifunctional catalysis of ORR and OER. SEM images of stainless steel mesh (b) prior to the growth and (c) densely coated by $Co_3O_4$ NWs. (d) Galvanodynamic discharge and charge polarization curves of $Co_3O_4$ NWs (SS: stainless steel mesh, GDL: carbon gas diffusion layer). (e) Galvanostatic pulse cycling at 50 mA of $Co_3O_4$ NWs on stainless steel mesh. Reproduced from Ref. [50] with permission from the John Wiley & Sons, Inc.

array electrode configuration and *in situ* carbon incorporation, which lead to the large active surface areas, enhanced mass/charge transport capability, and strong structural stability. Moreover, it can also efficiently catalyze the ORR process with strong methanol tolerance (Fig. 2d), featuring a desirable four-electron pathway for reversible ORR and OER. That makes it highly potential for the use in rechargeable metal-air batteries and regenerative fuel cells.

Besides 2D metal foils, self-supported catalysts are also designed by incorporating active species into the 3D scaffolds such as nickel foams and stainless steel meshes, which can enhance electroactivity

by providing high catalyst loading, smooth mass transfer and well electrode contact in the 3D networks. Metal oxides, mixed metal oxides and their composites have been grown or deposited onto Ni foams. For instance, Liang *et al.* deposited the composite of $Co_3O_4$/N-doped graphene on Ni foams to achieve a catalyst loading of 1.0 mg $cm^{-2}$ [47], much higher than that being coated on glassy carbon electrodes (0.1 mg $cm^{-2}$). The synthesized self-supported electrocatalyst could deliver a 10 mA $cm^{-2}$ current density for the OER process at a low overpotential of ~0.31 V with a small Tafel slope of 67 mV $decade^{-1}$, comparable to that of the best $Co_3O_4$-based catalysts at the same loading [48]. Moreover, NW arrays of Co/Ni mixed oxides freely standing on Ni foams were prepared through a hydrothermal route without using any template [49]. The Ni content had great influence on the morphology of the resultant electrocatalysts as well as their OER performance. Specifically, the morphology of mixed oxides was converted from NW to nanoflake arrays with the increase of Ni/Co molar ratios. The well-structured NW arrays, prepared at a Ni/Co molar ratio of 1:1, exhibited better OER activity than the NW arrays with other compositions.

Another widely used 3D substrate is stainless steel mesh, on which Lee *et al.* grew $Co_3O_4$ NWs using $Co(NO_3)_2$ precursor through a template-free hydrothermal method in alkaline solution (Fig. 3a) [50]. The obtained hierarchically mesoporous $Co_3O_4$ NWs with rounded outline and a circular hollow center adhered densely to stainless steel mesh in random directions (Fig. 3b,c). The resultant materials could perform as bifunctional catalysts for both ORR and OER. More importantly, they could be directly used as the cathode for rechargeable zinc-air batteries. Stainless steel mesh not only acts as the support for $Co_3O_4$ NW growth but also plays the role of a current collector without using ancillary binders, simplifying the battery design, and thereby significantly reducing internal resistance and prolonging lifetime of zinc-air batteries. In comparison to conventional cathodes composed of powdery catalysts coated on carbon gas diffusion layer (GDL), $Co_3O_4$ NWs growing on stainless steel mesh showed lower charge and discharge overpotentials at high currents beyond 20 mA $cm^{-2}$ (Fig. 3d). Notably, after 100 pulse cycles (500 min), the charge and discharge potentials remained unchanged, while even after 1500 pulse cycles, only a slight drop in the discharge potential was observed, which demonstrated the excellent rechargeability of the constructed batteries containing self-supported electrocatalysts (Fig. 3e).

In addition to metallic substrates, electroactive species can also grow on other rigid substrates such as graphite plates and glass sheets [51], affording controllable morphologies including nanowires/plates/pillars, etc., while various electroactive materials can replace metal oxides for specific catalytic reactions. For example, FeP [52] and $CoS_2$ [51] NW arrays growing on metal foils were reported to show exceptionally high catalytic activity and good durability for HER in electrochemical water splitting, potentially useful for large-scale hydrogen fuel production. Although rigid substrates have many advantages, their heavy and bulky configuration restricts materials synthesis by the size of reactors (e.g. autoclaves, tube furnaces), and can also result in the lack of flexibility of obtained electrocatalysts.

## Electrocatalysts growing on flexible substrates

Recyclable, environmental-friendly and easily processable carbon fiber paper (CFP), a soft current collector with high electron conductivity and robust mechanical stability, has been employed as the replacement of rigid metallic substrates [53]. The CFP, showing a 3D network composed of carbon fibers with a diameter of 7–10 μm, is commercially available, or can be self-made by carbonizing cellulose fiber paper [54,55]. Notably, the hydrophobic surface of pristine CFP needs to be converted to hydrophilic before use by certain surface treatment techniques such as mild oxidation and oxygen plasma, in order to facilitate the grown of non-metal or metal-containing electroactive materials [56].

Flexible non-metal self-supported electrocatalysts of phosphorus-doped graphitic carbon nitrides (g-$C_3N_4$) growing on CFP were reported to reversibly catalyze ORR and OER [55]. In the preparation, CFP was first mildly oxidized, creating abundant surface functional groups (e.g. $-COO^-$) to enhance its interaction with melamine as the N source and ethylene diphosphonic acid as the P source. After self-assembly and carbonization, P-doped g-$C_3N_4$ growing on CFP was obtained (PCN-CFP). Large pieces of self-supported catalysts, for example, a 10 cm × 15 cm sized PCN-CFP with high flexibility (Fig. 4a), could be produced by this method, where flower-like P-g-$C_3N_4$ densely grew on the CFP to produce porous frameworks (Fig. 4b). As a result of N, P dual action, the enhanced mass/charge transfer and high active surface areas owing to the 3D CFP framework and flower-like nanostructures, the bifunctional PCN-CFP could catalyze both ORR and OER, exhibiting superior activity, stability and reversibility over its powdery counterpart, undoped g-$C_3N_4$ growing on CFP or Pt supported on CFP. Another significant advantage of CFP-based self-supported catalysts is their flexibility, shape conformability and miniaturization, which enables their applications in foldable, bendable, portable and even wearable devices [57–59]. In the case of PCN-CFP, even after folded for three times, 91.3% of the initial ORR current and 94.6% of the initial OER current were maintained; the highly rolled-up PCN-CFP was capable of preserving 87.8% of the ORR current and 92.7% of the OER current (Fig. 4c). The flexible nature of PCN-CFP allows its direct use as the cathodes in zinc-air batteries, featuring low charge/discharge overpotential and long lifetime, comparable to commercial zinc-air batteries equipped with Pt electrodes.

Other than non-metal species, different metal-containing components have also been incorporated onto CFP. Kong *et al.* developed a facile two-step synthetic approach to prepare $CoSe_2$ catalysts by growing cobalt oxide nanoparticles on CFP, followed by selenization in Se vapour [53]. The self-supported $CoSe_2$ nanoparticulate films on CFP with cubic pyrite-type and orthorhombic macarsite-type crystalline structures (Fig. 4d) were obtained ($CoSe_2$ NP/CP), exhibiting outstanding HER activity, that is, a small Tafel slope of ~40 mV $decade^{-1}$ and an overpotential of ~180 mV to deliver a 100 mA $cm^{-2}$ current density in acidic solution, which largely outperformed $CoSe_2$ nanoparticles or films coated on glassy carbon electrodes (Fig. 4e). Further, the strong durability of $CoSe_2$ NP/CP was revealed by its capability of driving high catalytic currents at low and stable overpotentials over an extended period (Fig. 4f). Notably, benefiting from the outstanding chemical stability of carbon fibers, CFP-based self-supported catalysts can well perform under different pH values. Through low-temperature phosphidation of Co(OH)F, porous CoP NW arrays growing on CFP were prepared, acting as a robust and flexible HER catalyst, which could work efficiently over a broad pH range from 0 to 14

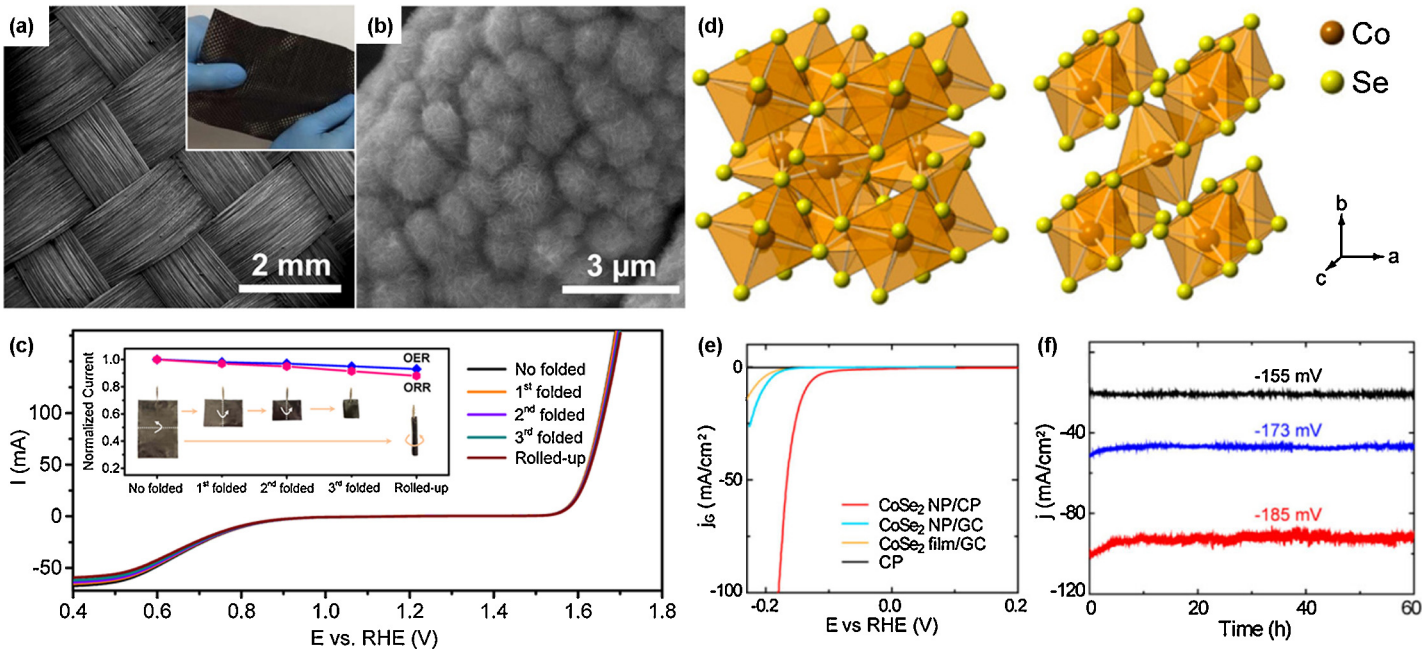


**FIGURE 4**

(a,b) SEM images and (inset in panel a) photograph of P-doped g-$C_3N_4$ growing on CFP (PCN-CFP). (c) Polarization curves of PCN–CFP in different folded and rolled-up forms, and (inset in panel c) variations of ORR (at 0.40 V) and OER (at 1.63 V) currents. Reproduced from Ref. [55] with permission from the John Wiley & Sons, Inc. (d) Crystal structure of $CoSe_2$ in (left) cubic pyrite-type phase and (right) orthorhombic macarsite-type phase. (e) Polarization curve for the HER in 0.5 M $H_2SO_4$ ($CoSe_2$ NP/CP: $CoSe_2$ nanoparticles growing on carbon fiber paper, $CoSe_2$ NP/GC: $CoSe_2$ nanoparticles coated on glassy carbon, $CoSe_2$ film/GC: $CoSe_2$ film coated on glassy carbon). (f) Chronoamperometric response of $CoSe_2$ NP/CP. Reproduced from Ref. [53] with permission from the American Chemical Society.

[24]. For instance, it showed a small Tafel slope of 51 mV decade$^{-1}$, a low and stable overpotential of 204 mV to deliver a 100 mA cm$^{-2}$ current density for at least 20 hours in acidic solution. Therefore, the significance of CFP as shown in above illustrations is of supplying a durable and flexible matrix, expanding surface areas to increase electroactive sites, enhancing the electron/charge transfer, and altering the electronic structures of electroactive species in some cases to modify their surface adsorbing/reacting property [24,55].

## Free-standing electrocatalyst films

Continuous evolution of a large amount of gas is usually involved in energy conversion processes, such as electrolytic water splitting ($2H_2O \rightarrow 2H_2 + O_2$) [60–62]. Since the hydrogen and oxygen bubbles are intrinsically insulative, they can block the flow of electrons/ions in electrochemical cells and result in substantial performance loss. Therefore, the design of highly throughput gas-breathing OER and HER catalysts for efficient gas evolution becomes critical [63–67]. Conventional powdery OER and HER catalysts coated on planar substrates (e.g. glassy carbon) usually form irregularly aggregated voids on electrodes that are unfavorable for gas transport (Fig. 5a), leading to inferior reaction kinetics and low catalyst durability. Very recently, a new class of free-standing films has been reported, which was composed of graphene sheets and its analogues (e.g. $MoS_2$, $WS_2$, g-$C_3N_4$) as the active species. Their ordered assembly can generate oriented transport channels with interconnected porosities, which are beneficial to $H_2$ and $O_2$ evolution (Fig. 5b). The film assembly was achieved by vacuum filtration of the mixed dispersion of graphene (usually reduced graphene oxide prepared by Hummer's method) and its analogues, in which the nanosheet species were prone to lie down on the surface of filter membrane under a directional flow caused by vacuum suction, and the film thickness was controlled by changing the concentration and volume of the initial dispersion. The interactions within hybrid sheets include attractive π–π stacking interaction (due to the graphitic domains of graphene) and repulsive electrostatic force (due to the carboxyl and hydroxyl groups of graphene) [68], which form an elaborate equilibrium in the film. Free-standing films can be finally obtained by peeling off from the filter membrane or by dissolving the filter membrane.

Different non-metal species can be integrated into the free-standing graphene films. Chen *et al.* reported a layer-by-layer assembly of graphene with intrinsic oxygen impurities and carbon nanotubes (CNTs) through the vacuum filtration method followed by N-doping with ammonia [69], affording a N,O-dual doped graphene-CNT film (NG-CNT), capable of efficiently catalyzing OER for water splitting (Fig. 6a). Containing >90 wt% of water

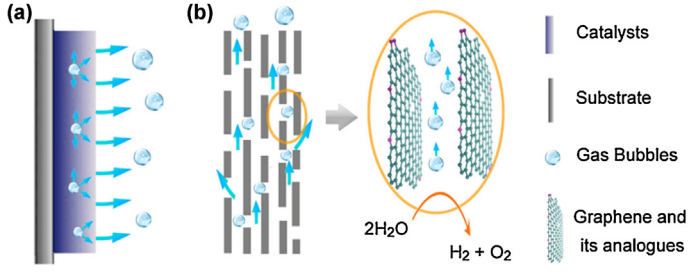


**FIGURE 5**

Schematic gas evolution in (a) powdery catalysts coated on planar substrates like glassy carbon, and (b) free-standing graphene-based films.

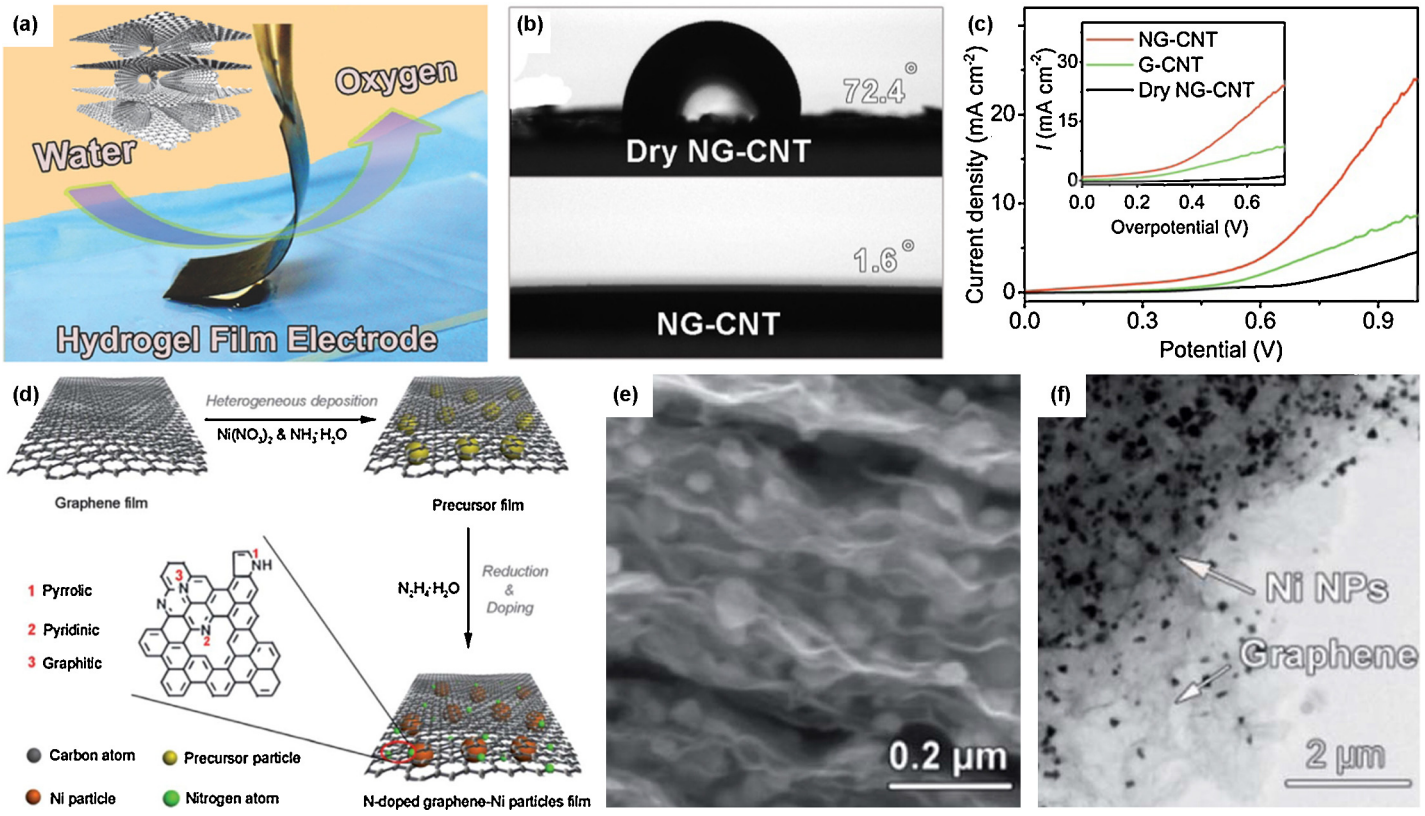


**FIGURE 6**

(a) Photograph of N,O-dual doped graphene-carbon nanotube films (NG-CNT) for water splitting. (b) Contact angles of NG-CNT and dry NG-CNT. (c) Polarization curves of NG-CNT, dry NG-CNT and G-CNT (undoped graphene-CNT film) in 0.1 M KOH. Reproduced from Ref. [69] with permission from the John Wiley & Sons, Inc. (d) Fabrication of nickel nanoparticles confined in N-doped graphene film (Ni–NG). (e) SEM and (f) TEM images of the Ni–NG. Reproduced from Ref. [79] with permission from the Royal Chemical Society.

with numerous carboxyl and epoxyl groups, NG-CNT was highly hydrophilic showing a small contact angle of 1.6° in contrast to 74.2° of dried NG-CNT (Fig. 6b), which endowed NG-CNT films with good wettability for the smooth access of electrolytes, largely benefiting the reaction kinetics. The dual active sites, C–N and C–O–C introduced by N and O doping, can provide abundant catalytic sites for OER. Thus, the NG-CNT film can deliver a 5 mA $cm^{-2}$ current density at an overpotential of 368 mV, better than that of dry NG-CNT film, undoped G-CNT film, and $IrO_2$ powders supported on glassy carbon electrodes (Fig. 6c). Since N doping can efficiently enhance the electroactivity of carbon-based materials [70–72], g-$C_3N_4$ with a high N content of up to 60 wt% [73–75] was also utilized to fabricate free-standing films with graphene. Porous g-$C_3N_4$ nanolayers were layer-by-layer assembled with N-doped graphene, rendering a flexible self-supported film (PCN@N-graphene) [76]. Inside the film, there were plenty of in-plane and out-of-plane pores ranging from tens of nanometers to several micrometers, originating from the cross-linking of graphene sheets and porous g-$C_3N_4$. The obtained materials can be directly utilized as the working electrode to catalyze HER, displaying a high exchange current density of 0.43 mA $cm^{-2}$ with a comparable onset potential to that of commercial Pt (a small gap of 8 mV) [77,78].

Free-standing graphene films can also interface with transition-metal molecular clusters through chemically/electrochemically deposition to further enhance the catalytic activity. It is feasible because the reduced graphene oxides prepared by Hummer's method have many defects, fragments and surface functional groups (epoxy, carboxyl and hydroxyl), which can act as the anchoring sites for metal, metal hydroxide and metal oxide clusters, facilitating their well dispersion [68]. Ni nanoparticles confined in N-doped graphene films (Ni-NG) were synthesized through a heterogeneous reaction from the $Ni(NO_3)_2$ precursor [79], followed by liquid-phase N doping using $N_2H_4$, which also reduced Ni species (Fig. 6d). The graphene sheets and Ni particles assembled into a well-organized hybrid film with lamellar structures (Fig. 6e), and the Ni particles with an average diameter of ~66 nm decorated on both sheet edges and base planes of graphene (Fig. 6f). The obtained free-standing hybrid films were directly used for catalyzing OER without any substrate, showing comparable activity to $IrO_2$. Similarly, if metal precursors were deposited on graphene sheets in alkaline solution such as urea without reduction, metal hydroxide-involved catalyst films could be synthesized, for example, NiCo double hydroxide decorated N-doped graphene films that were reported to act as efficient water splitting catalysts [80]. Further, metal oxides confined in graphene sheets could be obtained if the precursors were annealed in air. For example, a paper-like electrocatalyst film consisting of N-doped graphene-$NiCo_2O_4$ has been synthesized [81]. Its large surface area and pore volume originating from the advanced hierarchical porosity led to improved mass transfer and favorable kinetics, while the well dispersed $NiCo_2O_4$ strongly

interacting with N dopants in graphene afforded abundant electroactive sites.

Aforementioned facts indicate that the N dopant in graphene-based free-standing films is significant in promoting their electrocatalytic performance. For non-metal films, N doping is expected to improve the durability and stability of carbon catalysts due to an enhanced π–π stacking interaction [82,83]. The presence of N can also enhance the electron donor–acceptor property and consequently improve catalytic activity for specific reactions. For metal-containing films, N doping favors the affinity between graphene hosts and metal precursors, and thus leads to the well dispersion of resultant metal clusters. More importantly, owing to the high electronegativity of N, the strong interaction between doped nitrogen and metal centers, forming metal–N–C bonds in the hybrid films, may further boost the electrochemical processes [80].

## Concluding remarks

Recent advances on self-supported electrocatalysts were highlighted in this review, represented by metal oxide and metal oxide/carbon hybrid nanowires growing on rigid metallic substrates, carbon nitride and metal selenide/phosphide growing on flexible carbon fiber papers, as well as graphene and its analogue based free-standing porous films. These self-supported materials are capable of efficiently catalyzing ORR, OER and/or HER processes, and can be directly equipped in metal-air batteries. Although they appear to be highly promising, more work should be launched from materials, electrodes to devices, specifically described as follows. (i) Developing reliable materials with improved electrochemical performance is essential for the construction of self-supported catalysts. Both nano-morphology engineering and chemical component adjustment should be taken into account to achieve this goal. Besides simple patterns, hierarchical architectures with more complex geometry should be developed, introducing larger active surface areas, more exposed electroactive species and promoted mass transfer capability. Metals, non-metals and their composite materials should be selectively recruited to explore their synergistic effect; (ii) Structural and mechanical stability of the fabricated electrodes is critical for realistic applications regarding long-term and cyclic use. The interaction between electroactive materials and rigid/soft substrates as well as the integrity of free-standing films need to be further enhanced by controlled growth and other suitable industrial production technologies, such as inkjet, screen printing and especially 3D printing to afford fully printable self-supported electrodes in a large-scale, low-cost and time-efficient fashion; (iii) To finally equip the energy conversion devices with self-supported catalysts, configuration of these devices should be optimized to assure the smooth function of electrodes/electrolytes, stabilize the packaging materials, and protect the full integrity of power sources under various working conditions. Flexible energy devices are a future trend of such research due to their unique properties. Additional features like stretchability and optical transparency may also be added to the self-supported electrocatalysts, providing multiple functions and expanding their applications.

## Acknowledgements

This work is financially supported by the Australian Research Council (ARC) through the Discovery Project programs (DP140104062 and DP130104459), and the Discovery Early Career Researcher Award (DE150101306).

### References

[1] M. Zhang, et al. Nat. Chem. 6 (2014) 362.
[2] R.F. Service, Science 324 (2009) 1257.
[3] M. Armand, J.M. Tarascon, Nature 451 (2008) 652.
[4] V.R. Stamenkovic, et al. Nat. Mater. 6 (2007) 241.
[5] V. Mazumder, et al. J. Am. Chem. Soc. 132 (2010) 7848.
[6] J.I. Jung, et al. Angew. Chem. Int. Ed. 53 (2014) 4582.
[7] M.G. Walter, et al. Chem. Rev. 110 (2010) 6446.
[8] Y. Zheng, Nat. Commun. 5 (2014) 3783.
[9] J. Suntivich, et al. Nat. Chem. 3 (2011) 546.
[10] Y. Liang, et al. J. Am. Chem. Soc. 134 (2012) 3517.
[11] Y.L. Zhao, et al. Proc. Natl. Acad. Sci. U. S. A. 109 (2012) 19569.
[12] H. Zhu, et al. Nano Lett. 13 (2013) 2947.
[13] T. Takeguchi, et al. J. Am. Chem. Soc. 135 (2013) 11125.
[14] H. Wang, et al. ACS Nano 8 (2014) 4940.
[15] R.K. Das, et al. ACS Nano 8 (2014) 8447.
[16] J. Wang, et al. Angew. Chem. Int. Ed. 52 (2013) 5248.
[17] S. Xin, et al. Acc. Chem. Res. 45 (2012) 1759.
[18] F.Y. Cheng, et al. Chem. Soc. Rev. 41 (2012) 2172.
[19] J. Kibsgaard, et al. J. Am. Chem. Soc. 134 (2012) 7758.
[20] X.Y. Lang, et al. Nat. Nanotechnol. 6 (2011) 232.
[21] K. Wang, et al. Small 10 (2014) 14.
[22] L. Shen, et al. Adv. Funct. Mater. 24 (2014) 2630.
[23] Y. Jiang, et al. Nano Lett. 14 (2014) 365.
[24] J.Q. Tian, et al. J. Am. Chem. Soc. 136 (2014) 7587.
[25] J.Y. Liao, et al. Nano Lett. 13 (2013) 5467.
[26] C. Yuan, et al. Energy Environ. Sci. 5 (2012) 7883.
[27] J. Jiang, et al. Adv. Mater. 24 (2012) 5166.
[28] K. Gong, et al. Science 323 (2009) 760.
[29] Y. Liang, et al. J. Am. Chem. Soc. 135 (2013) 2013.
[30] M.K. Debe, Nature 486 (2012) 43.
[31] A.S. Aricò, et al. Nat. Mater. 4 (2005) 366.
[32] I.E.L. Stephens, et al. Energy Environ. Sci. 5 (2012) 6744.
[33] J.K. Nørskov, et al. Chem. Soc. Rev. 37 (2008) 2163.
[34] X. Wang, et al. Adv. Mater. 26 (2014) 4763.
[35] L. Li, et al. Energy Environ. Sci. 7 (2014) 2101.
[36] W. Zeng, et al. Adv. Mater. 26 (2014) 5310.
[37] V. Artero, et al. Angew. Chem. Int. Ed. 50 (2011) 7238.
[38] B. Cui, et al. Adv. Funct. Mater. 18 (2008) 1440.
[39] B.S. Yeo, A.T. Bell, J. Am. Chem. Soc. 133 (2011) 5587.
[40] H. Over, Chem. Rev. 112 (2012) 3356.
[41] Y. Lee, et al. J. Phys. Chem. Lett. 3 (2012) 399.
[42] Y. Li, et al. Adv. Mater. 22 (2010) 1926.
[43] X. Liu, et al. Chem. Mater. 26 (2014) 1889.
[44] T.Y. Ma, et al. J. Am. Chem. Soc. 136 (2014) 13925.
[45] J.A. Kaduk, J.A. Hanko, J. Appl. Crystallogr. 34 (2001) 710.
[46] J.K. Sun, Q. Xu, Energy Environ. Sci. 7 (2014) 2071.
[47] Y. Liang, et al. Nat. Mater. 10 (2011) 780.
[48] A.J. Esswein, et al. J. Phys. Chem. C 113 (2009) 15068.
[49] B. Lu, et al. Int. J. Hydrogen Energy 36 (2011) 72.
[50] D.U. Lee, et al. Adv. Energy Mater. 4 (2014) 1301389.
[51] M.S. Faber, et al. J. Am. Chem. Soc. 136 (2014) 10053.
[52] P. Jiang, et al. Angew. Chem. Int. Ed. 53 (2014) 12855.
[53] D. Kong, et al. J. Am. Chem. Soc. 136 (2014) 4897.
[54] L. Liu, et al. Adv. Mater. 26 (2014) 4855.
[55] T.Y. Ma, et al. Angew. Chem. Int. Ed. 54 (2015) 4646.
[56] M. Gong, et al. J. Am. Chem. Soc. 135 (2013) 8452.
[57] B. Liu, et al. Nano Lett. 12 (2012) 3005.
[58] Y. Wang, et al. Adv. Energy Mater. 5 (2015) 1400463.
[59] S. Tominaka, et al. Energy Environ. Sci. 2 (2009) 1074.
[60] R. Subbaraman, et al. Science 334 (2011) 1256.
[61] H.B. Gray, Nat. Chem. 1 (2009) 7.
[62] M.W. Kanan, D.G. Nocera, Science 321 (2008) 1072.
[63] S.K. Mazloomi, N. Sulaiman, Renew. Sustain. Energy Rev. 16 (2012) 4257.
[64] C. Brussieux, et al. Electrochim. Acta 56 (2011) 7194.
[65] M. Wang, et al. Int. J. Hydrogen Energy 35 (2010) 3198.
[66] S.D. Li, et al. Electrochim. Acta 54 (2009) 3877.
[67] E. Mirzakulova, et al. Nat. Chem. 4 (2012) 794.
[68] D. Li, et al. Nat. Nanotechnol. 3 (2008) 101.

[69] S. Chen, et al. Adv. Mater. 26 (2014) 2925.
[70] Y. Zheng, et al. J. Am. Chem. Soc. 133 (2011) 20116.
[71] T.Y. Ma, et al. Angew. Chem. Int. Ed. 53 (2014) 7281.
[72] J. Liang, et al. Angew. Chem. Int. Ed. 51 (2012) 3892.
[73] A. Thomas, et al. J. Mater. Chem. 18 (2008) 4893.
[74] Y. Wang, et al. Angew. Chem. Int. Ed. 51 (2012) 68.
[75] T.Y. Ma, et al. Small 10 (2014) 2382.
[76] J.J. Duan, et al. ACS Nano 9 (2015) 931.
[77] E. Navarro-Flores, et al. J. Mol. Catal. A: Chem. 226 (2005) 179.
[78] A.B. Laursen, et al. J. Chem. Educ. 89 (2012) 1595.
[79] S. Chen, et al. Energy Environ. Sci. 6 (2013) 3693.
[80] S. Chen, et al. Angew. Chem. Int. Ed. 52 (2013) 13567.
[81] S. Chen, S.Z. Qiao, ACS Nano 7 (2013) 10190.
[82] Y. Jiao, et al. J. Am. Chem. Soc. 136 (2014) 4394.
[83] H. Wang, H. Dai, Chem. Soc. Rev. 42 (2013) 3088.